

NUCLEAR MAGNETIC RESONANCE SPECTROSCOPY: AN EXPERIMENTALLY ACCESSIBLE PARADIGM FOR QUANTUM COMPUTING*

David G. Cory and Mark D. Price

Nuclear Engineering, Massachusetts Institute of Technology, Cambridge, MA
02139, USA

Amr F. Fahmy and Timothy F. Havel[†]

Biological Chemistry and Molecular Pharmacology, Harvard Medical School,
Boston, MA 02115, USA

Submitted to Physica D, January 17, 1997; Accepted August 27, 1997

(PACS codes: 05.30.-d, 75.45.+j, 76.70.Fz, 89.80.+h)

* Expanded version of speech presented to the Fourth Workshop on Physics and Computation, Boston University, November 24, 1996.

[†] To whom correspondence should be addressed at havel@euclid.med.harvard.edu.

ABSTRACT

We present experimental results which demonstrate that nuclear magnetic resonance spectroscopy is capable of efficiently emulating many of the capabilities of quantum computers, including unitary evolution and coherent superpositions, but without attendant wave-function collapse. This emulation is made possible by two facts.

The first is that the spin active nuclei in each molecule of a liquid sample are largely isolated from the spins in all other molecules, so that each molecule is effectively an independent quantum computer. The second is the existence of a manifold of statistical spin states, called *pseudo-pure* states, whose transformation properties are identical to those of true pure states. These facts enable us to operate on coherent superpositions over the spins in each molecule using full quantum parallelism, and to combine the results into deterministic macroscopic observables via thermodynamic averaging. We call a device based on these principles an *ensemble quantum computer*.

Our results show that it is indeed possible to prepare a pseudo-pure state in a macroscopic liquid sample under ambient conditions, to transform it into a coherent superposition, to apply elementary quantum logic gates to this superposition, and to convert it into the equivalent of an entangled state. Specifically, we have:

- Implemented the quantum XOR gate in two different ways, one using Pound-Overhauser double resonance, and the other using a spin-coherence double resonance pulse sequence.
- Demonstrated that the square root of the Pound-Overhauser XOR corresponds to a conditional rotation, thus obtaining a universal set of gates.
- Devised a spin-coherence implementation of the Toffoli gate, and confirmed that it transforms the equilibrium state of a four-spin system as expected.
- Used standard gradient-pulse techniques in NMR to equalize all but one of the populations in a two-spin system, so obtaining the pseudo-pure state that corresponds to $|00\rangle$.
- Validated that one can identify which basic pseudo-pure state is present by transforming it into one-spin superpositions, whose associated spectra jointly characterize the state.
- Applied the spin-coherence XOR gate to a one-spin superposition to create an entangled state, and confirmed its existence by detecting the associated double-quantum coherence via gradient-echo methods.

1 Introduction

The theory of quantum computing is advancing at a rate that vastly outstrips its experimental realization (for accounts, see [1, 2, 6]). Most attempts to implement a quantum computer have utilized submicroscopic assemblies of quantum spins, which are difficult to prepare, isolate, manipulate and observe. A “homologous” system that exhibits many of the same properties, but is easier to work with, would clearly be very useful both as a means of testing the theoretical predictions, and exploring implementation issues like error correction. Such a system is provided by weakly polarized macroscopic ensembles of spins, which are readily manipulated and observed by *nuclear magnetic resonance spectroscopy*, or NMR.

The spins of a molecule in solution are largely isolated from their surroundings by simple surface-to-volume considerations, and from the spins in neighboring molecules by diffusional motion, which averages their dipole-dipole coupling to a second-order effect [14]. This fact enables us to work with a *reduced density matrix* Ψ of size 2^n , where n is the number of spin $\frac{1}{2}$ nuclei in the molecule, rather than 2^N where N is the total number of such spins in the sample [11]. It is also customary in NMR spectroscopy to shift the reduced density matrix by subtraction of its mean trace, since only the traceless part undergoes unitary evolution, and to scale it to have integral elements [7]. In the next paragraph, we define a manifold of statistical spin states with a reduced density matrix whose traceless part is proportional to the traceless part of the usual density matrix of a pure state.

Henceforth, whenever we use the term “density matrix”, we mean “reduced, shifted and scaled density matrix” unless otherwise stated. When such a density matrix has rank equal to one (after adding an appropriate multiple of the unit matrix to it), it can be factored into a dyadic product of the coordinates of a “spinor” and its conjugate versus the usual \mathbf{I}_z basis, and this factorization is unique up to an overall phase factor. This mapping between spinor coordinates and density matrices that can be shifted to a signature of $[\pm 1, 0, \dots, 0]$ is *covariant*, in the sense that if we apply a unitary matrix to the spinor’s coordinates, the corresponding density matrix transforms by conjugation with the *same* unitary matrix. As a result, we can regard such a density matrix as a kind of spinor, and perform essentially arbitrary unitary transformations on it via NMR spectroscopy, thereby “emulating” a quantum computer. We shall call the states described by density matrices with $2^n - 1$ equal eigenvalues “pseudo-pure” states, and the corresponding spinors “pseudo-spinors”.

Of course, some things are lost in translation. For example, the density matrix is not changed on rotation by 2π , although spinors change sign. Since these sign changes cannot easily be observed, this seems to be of little consequence for quantum computing. More important is the fact that the “coherence” observed by NMR spectroscopy is always an ensemble average over an astronomical number of microscopic quantum systems. As a consequence, the NMR spectrum of a pseudo-pure state yields the expectation values of certain observables relative to the corresponding pseudo-spinor, rather than a random eigenvalue of one

of them. In particular, *wave function collapse does not occur*. A variety of other more easily controlled “filtering” mechanisms are available in NMR spectroscopy, however, and we have shown that for most computational purposes the ability to measure expectation values directly is actually a great advantage [5]. NMR experiments on liquid samples possess a number of other highly desirable features as well; in particular, the decoherence times are typically on the order of seconds.

NMR spectroscopy in fact provides a means of building a nonconventional computer that can be programmed much like a quantum computer, but is much easier to implement on at least a limited scale. In some respects, this approach also resembles DNA computing, in that it can use the parallelism inherent in ensembles of molecules to efficiently count the number of solutions to combinatorial problems, trading an exponential growth in the time required against an exponential growth in the sample size. More generally, we have called a computational device that operates by running a large number of quantum computers on coherent superpositions, and then estimates the expectation values of observables by summing them over all the quantum computers, an *ensemble quantum computer*. A detailed introduction to the theory of such machines may be found in [5]; this paper will describe how basic quantum logic gates can be implemented via NMR spectroscopy, and present experimental results to validate our claims. After the majority of these results had been obtained [4], we learned of a similar approach proposed by other researchers [9, 10].

2 Basic techniques from NMR

This section introduces the basic techniques from NMR spectroscopy that are needed for this paper, and in the process defines the notation it uses (for more complete introductions, see e.g. [3, 8, 13]).

Let us consider the simplest nontrivial case, which contains all the essential ingredients of solution NMR spectroscopy. This is a liquid consisting of identical molecules each containing exactly two coupled spin $\frac{1}{2}$ nuclei of the same isotope (throughout this paper, ^1H). The dipolar coupling between the spins is averaged to zero by the rotational motion of the molecules in the liquid, and hence the coupling in this case is the so-called *scalar coupling*, which is mediated by electron correlation in the chemical bonds linking the atoms. It will simplify our presentation if we assume *weak coupling*, i.e. that the coupling constant J_{12} is small compared to the difference $|\omega_1 - \omega_2|$ in the resonance frequencies of the two spins. With the convention that the magnetic field is along the z -axis, the Hamiltonian of this system is $\mathbf{H} = \omega_1 \mathbf{I}_z^1 + \omega_2 \mathbf{I}_z^2 + 2\pi J_{12} \mathbf{I}_z^1 \mathbf{I}_z^2$, where \mathbf{I}_z^k ($k = 1, 2$) are the usual matrices for the z -component of the angular momentum of the spins. Because the energy level differences are small compared to kT at room temperature, the equilibrium density matrix of this system is given to an excellent approximation by $\text{Exp}(-\mathbf{H}/kT) \approx \mathbf{1} - \mathbf{H}/kT$. On taking account of the fact that $|J_{12}| \ll \omega_1 \approx \omega_2$, removing the trace and scaling, the equilibrium

density matrix becomes

$$\Psi_{eq} = \mathbf{I}_z^1 + \mathbf{I}_z^2 = \begin{pmatrix} 1 & 0 & 0 & 0 \\ 0 & 0 & 0 & 0 \\ 0 & 0 & 0 & 0 \\ 0 & 0 & 0 & -1 \end{pmatrix} \begin{array}{c} \downarrow\downarrow \\ \downarrow\uparrow \\ \uparrow\downarrow \\ \uparrow\uparrow \end{array} \quad (1)$$

(where the longitudinal spin states which label the rows and columns of this matrix are shown along its right-hand side).

Rather than writing them out explicitly, NMR spectroscopists typically represent their density matrices as linear combinations of “product operators”, i.e. products of the usual angular momentum operators \mathbf{I}_x^k , \mathbf{I}_y^k , \mathbf{I}_z^k (as in Eq. (1)) [7, 13]. This makes it very easy to describe the unitary transformations effected by applying RF (radio-frequency) pulses to the sample. For example, a “soft” pulse whose frequency range spans the resonance frequency of only the first spin, and which imparts an energy sufficient to rotate that spin by an angle φ about the y -axis (in a frame rotating with the carrier of the receiver [7]) is

$$\mathbf{I}_z^1 \xrightarrow{[\varphi]_y^1} \cos(\varphi)\mathbf{I}_z^1 + \sin(\varphi)\mathbf{I}_x^1. \quad (2)$$

Thus when a “soft” (i.e. spin-selective) $[\pi/2]$ y -pulse is applied to the first spin of a two-spin system at equilibrium, we obtain $\mathbf{I}_x^1 + \mathbf{I}_z^2$, while a “hard” (nonselective) $[\pi/2]$ y -pulse yields $\mathbf{I}_x^1 + \mathbf{I}_x^2$.

The density matrix evolves according to the time-dependent unitary transformation [7]

$$\Psi \xrightarrow{t \mathbf{H}} \mathbf{Exp}(-i t \mathbf{H}) \Psi \mathbf{Exp}(i t \mathbf{H}). \quad (3)$$

Since all three terms of the Hamiltonian commute, the above propagator factors into a product of the chemical shift and scalar coupling propagators. The chemical shift propagator for the first spin can be expanded as

$$\mathbf{Exp}(i t \omega_1 \mathbf{I}_z^1) = \cos(\omega_1 t/2) \mathbf{1} + 2i \sin(\omega_1 t/2) \mathbf{I}_z^1. \quad (4)$$

An exercise in the Pauli matrix algebra then shows that

$$\mathbf{Exp}(-i t \omega_1 \mathbf{I}_z^1) \mathbf{I}_x^1 \mathbf{Exp}(i t \omega_1 \mathbf{I}_z^1) = \cos(\omega_1 t) \mathbf{I}_x^1 + \sin(\omega_1 t) \mathbf{I}_y^1. \quad (5)$$

Altogether, we obtain:

$$\begin{aligned} \mathbf{I}_x^1 &\xrightarrow{\omega_1 t \mathbf{I}_z^1} \cos(\omega_1 t) \mathbf{I}_x^1 + \sin(\omega_1 t) \mathbf{I}_y^1 \\ \mathbf{I}_y^1 &\xrightarrow{\omega_1 t \mathbf{I}_z^1} \cos(\omega_1 t) \mathbf{I}_y^1 - \sin(\omega_1 t) \mathbf{I}_x^1 \\ \mathbf{I}_z^1 &\xrightarrow{\omega_1 t \mathbf{I}_z^1} \mathbf{I}_z^1 \end{aligned} \quad (6)$$

This propagator has no effect on terms involving only the second spin, which evolve analogously under their own chemical shift Hamiltonian.

The scalar coupling propagator, on the other hand, is

$$\text{Exp}(2\pi i J_{12} t \mathbf{I}_z^1 \mathbf{I}_z^2) = \cos(\pi J_{12} t/2) \mathbf{1} + 4i \sin(\pi J_{12} t/2) \mathbf{I}_z^1 \mathbf{I}_z^2. \quad (7)$$

A similar calculation shows that it transforms the one-spin operators as follows:

$$\begin{aligned} \mathbf{I}_x^1 &\xrightarrow{2\pi J_{12} t \mathbf{I}_z^1 \mathbf{I}_z^2} \cos(\pi J_{12} t) \mathbf{I}_x^1 + 2 \sin(\pi J_{12} t) \mathbf{I}_y^1 \mathbf{I}_z^2 \\ \mathbf{I}_y^1 &\xrightarrow{2\pi J_{12} t \mathbf{I}_z^1 \mathbf{I}_z^2} \cos(\pi J_{12} t) \mathbf{I}_y^1 - 2 \sin(\pi J_{12} t) \mathbf{I}_x^1 \mathbf{I}_z^2 \\ \mathbf{I}_z^1 &\xrightarrow{2\pi J_{12} t \mathbf{I}_z^1 \mathbf{I}_z^2} \mathbf{I}_z^1 \end{aligned} \quad (8)$$

with analogous expressions for the terms \mathbf{I}_x^2 , \mathbf{I}_y^2 and \mathbf{I}_z^2 .

Physically, the above expressions describe the precession of the transverse magnetization about the applied field, which generates a rotating magnetic moment in the xy -plane. The complex-valued signal induced in the receiver is calculated by taking the trace of the product of this time-dependent density matrix with

$$\mathbf{I}_+^1 + \mathbf{I}_+^2 = \begin{pmatrix} 0 & 1 & 1 & 0 \\ 0 & 0 & 0 & 1 \\ 0 & 0 & 0 & 1 \\ 0 & 0 & 0 & 0 \end{pmatrix}, \quad (9)$$

where $\mathbf{I}_+^k = \mathbf{I}_x^k + i\mathbf{I}_y^k$ as usual (see e.g. [13]). Since this matrix contains only four nonzero elements, the spectrum contains direct information on only four of the ten independent elements of the density matrix, namely $\Psi_{12} = \Psi_{21}^*$, $\Psi_{13} = \Psi_{31}^*$, $\Psi_{24} = \Psi_{42}^*$ and $\Psi_{34} = \Psi_{43}^*$. These elements are called *single-quantum coherences*, because they connect pairs of states related by single spin flips (cf. Fig. 3).

For example, the signal due to the chemical shift precession of \mathbf{I}_x^1 alone is

$$\text{tr}(\mathbf{I}_+^1 (\cos(\omega_1 t) \mathbf{I}_x^1 + \sin(\omega_1 t) \mathbf{I}_y^1)) = \cos(\omega_1 t) + i \sin(\omega_1 t). \quad (10)$$

These two terms are modulated by the scalar coupling evolution to

$$\begin{aligned} &\cos(\omega_1 t) \text{tr}(\mathbf{I}_+^1 (\cos(\pi J_{12} t) \mathbf{I}_x^1 + 2 \sin(\pi J_{12} t) \mathbf{I}_y^1 \mathbf{I}_z^2)) \\ &= \cos(\omega_1 t) \cos(\pi J_{12} t) \\ &\sin(\omega_1 t) \text{tr}(\mathbf{I}_+^1 (\cos(\pi J_{12} t) \mathbf{I}_x^1 - 2 \sin(\pi J_{12} t) \mathbf{I}_x^1 \mathbf{I}_z^2)) \\ &= \sin(\omega_1 t) \cos(\pi J_{12} t). \end{aligned} \quad (11)$$

The total signal due to the first spin is thus

$$\begin{aligned} &\cos(\omega_1 t) \cos(\pi J_{12} t) + \sin(\omega_1 t) \cos(\pi J_{12} t) \\ &= \frac{1}{2} (\exp(i(\omega_1 - \pi J_{12})t) + \exp(i(\omega_1 + \pi J_{12})t)), \end{aligned} \quad (12)$$

which shows that the real part of the Fourier transform consists of a pair of peaks centered on the resonance frequency of the spin and separated by the

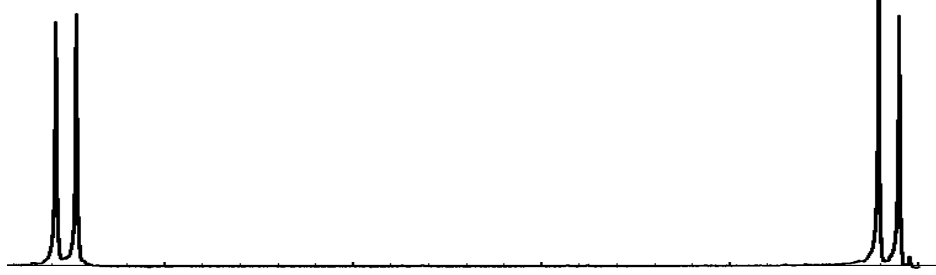


Figure 1: The experimental NMR spectrum of liquid 2,3-dibromo-thiophene (see below) in a 9.4 Tesla field, at which the two doublets are separated by 130 Hz. This spectrum was collected by applying a nonselective $[\pi/2]$ y -pulse to the equilibrium state and Fourier transforming the resulting signal (see text). Note that frequency (the horizontal axis) increases from right-to-left in NMR spectra.

coupling constant; this is called an *in-phase* doublet, meaning that both peaks have the same sign. Thus if the magnetization due to both spins is rotated into the transverse plane by a hard $[\pi/2]$ y -pulse, one obtains a spectrum containing a pair of doublets. This is shown in Fig. 1, using the molecule 2,3-dibromo-thiophene shown in Fig. 2.

Once the magnetization due to a spin has been placed in the transverse plane, a soft $[\pi]$ pulse in the middle of an evolution period t may be used to *refocus* its chemical shift evolution during that period, as follows:

$$\begin{aligned}
 \mathbf{I}_x^1 &\xrightarrow{\omega_1 t \mathbf{I}_z^1/2} \cos(\omega_1 t/2) \mathbf{I}_x^1 + \sin(\omega_1 t/2) \mathbf{I}_y^1 \\
 &\xrightarrow{[\pi]_y^1} -\cos(\omega_1 t/2) \mathbf{I}_x^1 + \sin(\omega_1 t/2) \mathbf{I}_y^1 \\
 &\xrightarrow{\omega_1 t \mathbf{I}_z^1/2} -\cos(\omega_1 t/2) (\cos(\omega_1 t/2) \mathbf{I}_x^1 + \sin(\omega_1 t/2) \mathbf{I}_y^1) \\
 &\quad + \sin(\omega_1 t/2) (\cos(\omega_1 t/2) \mathbf{I}_y^1 - \sin(\omega_1 t/2) \mathbf{I}_x^1)
 \end{aligned} \tag{13}$$

Standard trigonometric identities show that this last expression is simply $-\mathbf{I}_x^1$. Thus, up to an inconsequential overall phase factor, we have cancelled the effect of chemical shift evolution.

A very similar calculation shows that such a soft $[\pi]$ y -pulse also cancels the scalar coupling evolution, so that only the chemical shift evolution of the other spin occurs during the interval, i.e.

$$\begin{aligned}
 &\mathbf{I}_x^1 + \mathbf{I}_x^2 \\
 &\xrightarrow{t \mathbf{H}/2 - [\pi]_y^1 - t \mathbf{H}/2 - [\pi]_y^1} \mathbf{I}_x^1 + \cos(\omega_2 t) \mathbf{I}_x^2 + \sin(\omega_2 t) \mathbf{I}_y^2.
 \end{aligned} \tag{14}$$

We shall denote such a rotation of the second spin about the z -axis by $[\omega_2 t]_z^2$. Note, however, that $[\pi]_z^2$ is more easily obtained as $[\pi]_y^2 - [\pi]_x^2$ (a $[\pi]_y^2$ pulse immediately followed by a $[\pi]_x^2$).

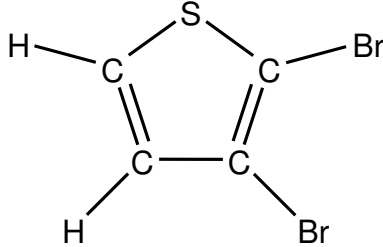


Figure 2: The chemical structure of 2,3-dibromo-thiophene. This molecule is a liquid at room temperature, and contains two inequivalent, spin $\frac{1}{2}$ hydrogen atoms with a coupling constant of 6.0 Hz.

A hard $[\pi]$ y -pulse applied in the middle of a period, on the other hand, cancels the chemical shift evolution of both spins while allowing their scalar coupling to evolve. This is because the pulse just changes the sign of the density matrix half-way through the period, i.e.

$$\begin{aligned}
 \mathbf{I}_x^1 &\xrightarrow{\pi J_{12}t \mathbf{I}_z^1 \mathbf{I}_z^2} \cos(\pi J_{12}t/2) \mathbf{I}_x^1 + 2 \sin(\pi J_{12}t/2) \mathbf{I}_y^1 \mathbf{I}_z^2 \\
 &\xrightarrow{[\pi]_y^{12}} -\cos(\pi J_{12}t/2) \mathbf{I}_x^1 - 2 \sin(\pi J_{12}t/2) \mathbf{I}_y^1 \mathbf{I}_z^2 \\
 &\xrightarrow{\pi J_{12}t \mathbf{I}_z^1 \mathbf{I}_z^2} -\cos(\pi J_{12}t) \mathbf{I}_x^1 - 2 \sin(\pi J_{12}t) \mathbf{I}_y^1 \mathbf{I}_z^2 ,
 \end{aligned} \tag{15}$$

thereby yielding the negative of what one would have obtained with no $[\pi]$ pulse (as shown). We will denote such a scalar coupling evolution, with no chemical shift evolution, by $[t]$.

A *gradient pulse* produces a transient field inhomogeneity along the z -axis, which has the Hamiltonian

$$\mathbf{H}_{\text{grad}} = \gamma \mathbf{r} \cdot \nabla B_z \tag{16}$$

where \mathbf{r} is the position vector within the sample. Although the microscopic evolution remains unitary (of course!), a gradient pulse dephases the macroscopic transverse magnetization due to the off-diagonal elements of the density matrix. The decay rate of each element is proportional to the difference in the number of “up” spins between the corresponding pair of states, which is commonly called the *coherence order*. The net effect is to zero the off-diagonal elements of the density matrix whose coherence order is nonzero, thus effecting a *projection* of the state.

This makes it possible to destroy (or more precisely, render unobservable) the magnetization due to selected spins with a combination of soft and gradient pulses, e.g.

$$\mathbf{I}_z^1 + \mathbf{I}_z^2 \xrightarrow{[\pi/2]_y^2} \mathbf{I}_z^1 + \mathbf{I}_x^2 \xrightarrow{[\text{grad}]_z} \mathbf{I}_z^1 . \tag{17}$$

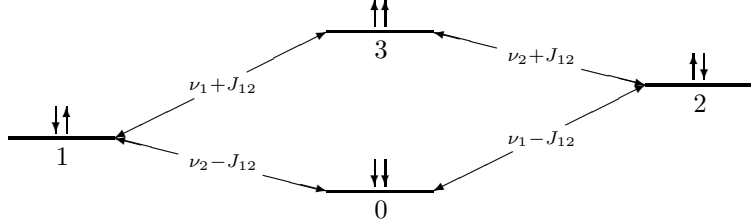


Figure 3: The energy level diagram for a coupled two-spin system, where the resonance frequencies of the two spins are ν_1 and ν_2 , while the coupling constant is J_{12} . The single-quantum transitions allowed by the selection rules for angular momentum are indicated by two-headed arrows, together with the energy associated with each.

A further $[\pi/2]$ y -pulse transforms the remaining term to \mathbf{I}_x^1 , which is converted by a scalar coupling evolution of $[1/(2J_{12})]$ to $2\mathbf{I}_y^1\mathbf{I}_z^2$, and thereafter evolves as

$$\begin{aligned} & \cos(\omega_1 t) (2 \cos(\pi J_{12} t) \mathbf{I}_y^1 \mathbf{I}_z^2 - \sin(\pi J_{12} t) \mathbf{I}_x^1) \\ & - \sin(\omega_1 t) (2 \cos(\pi J_{12} t) \mathbf{I}_x^1 \mathbf{I}_z^2 + \sin(\pi J_{12} t) \mathbf{I}_x^1) \end{aligned} \quad (18)$$

Taking the trace product of this with $\mathbf{I}_+^1 + \mathbf{I}_+^2$ yields the signal

$$\begin{aligned} & -\cos(\omega_1 t) \sin(\pi J_{12} t) - \sin(\omega_1 t) \sin(\pi J_{12} t) \\ & = \frac{1}{2} (\exp(i(\omega_1 - \pi J_{12}) t) - \exp(i(\omega_1 + \pi J_{12}) t)). \end{aligned} \quad (19)$$

Thus if one collects a spectrum starting after the $[1/(2J_{12})]$ evolution, one obtains an *anti-phase* doublet consisting of two peaks of opposite sign.

Alternatively, one can apply a selective $[-\pi/2]_x^2$ pulse to the second spin of $2\mathbf{I}_y^1\mathbf{I}_z^2$, obtaining the correlated state $2\mathbf{I}_y^1\mathbf{I}_y^2$, or a $[\pi/2]_y^2$ pulse to obtain $2\mathbf{I}_y^1\mathbf{I}_x^2$. These contain no single-quantum coherences, and hence produce no observable magnetization.

3 The Pound-Overhauser XOR and conditional rotation

The most obvious way to implement the quantum XOR (or controlled-NOT) gate is to use a pulse that is selective for just *one* component of a doublet; this effects a population transfer similar to the original ENDOR experiment, and constitutes an example of *Pound-Overhauser double resonance* [14]. Specifically, if we apply a $[\pi]$ pulse about the y -axis to the transitions $1 \leftrightarrow 3$ and $2 \leftrightarrow 3$ (see Fig. 3), we obtain an XOR gate with the output on the first and second spins, respectively. These pulses will be denoted by $[\pi]_y^{+k}$ ($k = 1, 2$). If $|\epsilon_1, \epsilon_2\rangle$

Product Operator	Initial Spectra		Final Spectra		Product Operator
	$[\pi/2]_y^1$	$[\pi/2]_y^2$	$[\pi/2]_y^1$	$[\pi/2]_y^2$	
\mathbf{I}_z^1					\mathbf{I}_z^1
\mathbf{I}_z^2					$2\mathbf{I}_z^1\mathbf{I}_z^2$
$2\mathbf{I}_z^1\mathbf{I}_z^2$					\mathbf{I}_z^2

Table 1: Simplified “stick” spectra for each of the three diagonal product operators that would be observed after selective $[\pi/2]_y^k$ observation pulses on the k -th spin, before (initial) and after (final) applying an XOR with its output on the second spin (see text).

denotes the spinor of a single state ($\epsilon_1, \epsilon_2 \in \{0, 1\}$), these pulses effect the unitary transformations of the density matrix of the corresponding pure state given by

$$\begin{aligned} \mathbf{U}_{\text{PO}}^{1\dagger} |\epsilon_1, \epsilon_2\rangle \langle \epsilon_1, \epsilon_2| \mathbf{U}_{\text{PO}}^1 &= |\epsilon_1 \oplus \epsilon_2, \epsilon_2\rangle \langle \epsilon_1 \oplus \epsilon_2, \epsilon_2| \\ \mathbf{U}_{\text{PO}}^{2\dagger} |\epsilon_1, \epsilon_2\rangle \langle \epsilon_1, \epsilon_2| \mathbf{U}_{\text{PO}}^2 &= |\epsilon_1, \epsilon_1 \oplus \epsilon_2\rangle \langle \epsilon_1, \epsilon_1 \oplus \epsilon_2|, \end{aligned} \quad (20)$$

where “ \oplus ” denotes the boolean XOR operation, and

$$\begin{aligned} \mathbf{U}_{\text{PO}}^1 &\equiv \begin{pmatrix} 1 & 0 & 0 & 0 \\ 0 & 0 & 0 & 1 \\ 0 & 0 & 1 & 0 \\ 0 & -1 & 0 & 0 \end{pmatrix} \\ \mathbf{U}_{\text{PO}}^2 &\equiv \begin{pmatrix} 1 & 0 & 0 & 0 \\ 0 & 1 & 0 & 0 \\ 0 & 0 & 0 & 1 \\ 0 & 0 & -1 & 0 \end{pmatrix}. \end{aligned} \quad (21)$$

By applying $[\pi]$ pulses to the transitions $0 \leftrightarrow 1$ and $0 \leftrightarrow 2$, we obtain the boolean operations $|\epsilon_1 \oplus \bar{\epsilon}_2, \epsilon_2\rangle$ and $|\epsilon_1, \bar{\epsilon}_1 \oplus \epsilon_2\rangle$ (where the overbar denotes the NOT of the corresponding qubit); these pulses will be denoted by $[\pi]_y^{-k}$ ($k = 1, 2$).

The necessary selectivity can be obtained with a long sinc-modulated pulse, whose Fourier transform has a square-wave envelope occupying just the width of a single peak. Based on the matrices in Eq. (21) above, the result of applying such a pulse to the first spin (i.e. the left-most peak in its doublet) of a two-spin

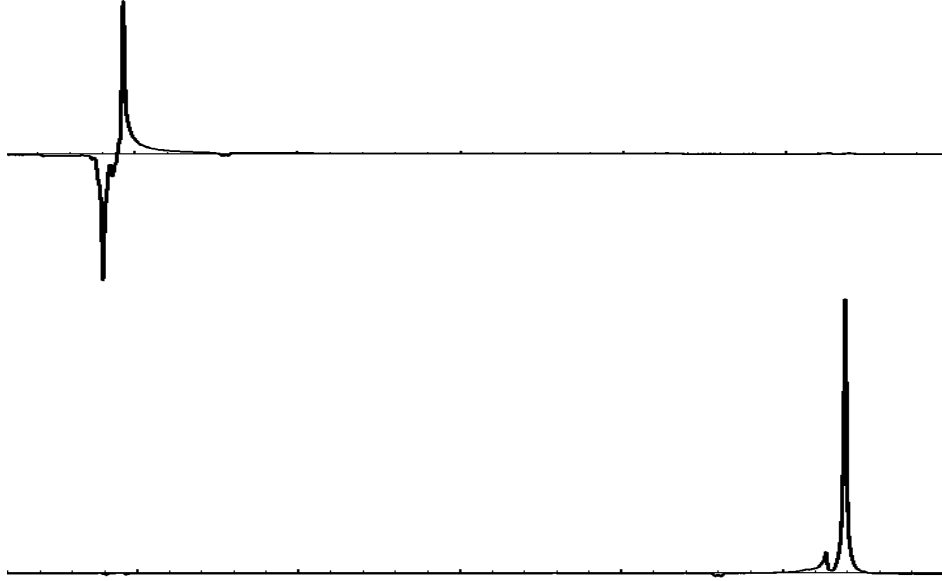


Figure 4: The spectra obtained from $[\pi/2]_y^k$ readout pulses on the first (above) and second (below) spins, following a $[\pi]_y^{+1}$ pulse applied to the equilibrium state (see text).

system at equilibrium should be

$$\begin{aligned}
 |00\rangle\langle 00| - |11\rangle\langle 11| &= \mathbf{I}_z^1 + \mathbf{I}_z^2 \\
 \xrightarrow{[\pi]_y^{+1}} \quad |00\rangle\langle 00| - |01\rangle\langle 01| &= 2\mathbf{I}_z^1\mathbf{I}_z^2 + \mathbf{I}_z^2 .
 \end{aligned} \tag{22}$$

This expectation can be confirmed by collecting spectra following ordinary soft readout pulses on each spin. The spectra expected from the individual product operators are shown in a diagrammatic “stick” form in Table 1, and the spectrum which results from any sum of these operators will be the point-by-point sum of the spectra from the individual terms in the sum. For example, a readout pulse on the second spin yields

$$2\mathbf{I}_z^1\mathbf{I}_z^2 + \mathbf{I}_z^2 \xrightarrow{[\pi/2]_y^2} 2\mathbf{I}_z^1\mathbf{I}_x^2 + \mathbf{I}_x^2 \tag{23}$$

Due to interference between the in-phase and anti-phase signals, the resulting spectrum contains only a single peak, with twice the intensity of the peaks one gets from a readout on the first spin, as shown in Fig. 4.

Similarly, the result of applying a Pound-Overhauser XOR to the second spin is $\mathbf{I}_z^1 + 2\mathbf{I}_z^1\mathbf{I}_z^2$. The effects of a Pound-Overhauser XOR on all the two-spin product operators are shown in Table 2. Note that the matrices in eq. (21) differ in the sign of one element from the matrices for the XOR usually encountered

*	$\frac{1}{2}\mathbf{1}$	\mathbf{I}_x^2	\mathbf{I}_y^2	\mathbf{I}_z^2
$\frac{1}{2}\mathbf{1}$	$\frac{1}{2}\mathbf{1}$	$-\mathbf{I}_y^1\mathbf{I}_y^2$	$\mathbf{I}_y^1\mathbf{I}_x^2$	\mathbf{I}_z^2
\mathbf{I}_x^1	$\mathbf{I}_x^1\mathbf{I}_z^2$	$-\mathbf{I}_z^1\mathbf{I}_x^2$	$-\mathbf{I}_z^1\mathbf{I}_y^2$	\mathbf{I}_x^1
\mathbf{I}_y^1	\mathbf{I}_y^1	$-\mathbf{I}_y^2$	\mathbf{I}_x^2	$\mathbf{I}_y^1\mathbf{I}_z^2$
\mathbf{I}_z^1	$\mathbf{I}_z^1\mathbf{I}_z^2$	$\mathbf{I}_x^1\mathbf{I}_x^2$	$\mathbf{I}_x^1\mathbf{I}_y^2$	\mathbf{I}_z^1

Table 2: The effect of the $[\pi]_y^{+1}$ pulse on all the product operators of a two-spin system. The two factors of the product operator on which the XOR acts are shown in the left column and top row, while the result is shown in the corresponding table cell. Thus for example, a $[\pi]_y^{+1}$ pulse converts the product operator \mathbf{I}_x^1 to $2\mathbf{I}_x^1\mathbf{I}_z^2$.

in quantum computing, e.g.

$$\mathbf{U}_{\text{QC}}^1 \equiv \begin{pmatrix} 1 & 0 & 0 & 0 \\ 0 & 0 & 0 & 1 \\ 0 & 0 & 1 & 0 \\ 0 & 1 & 0 & 0 \end{pmatrix}. \quad (24)$$

This sign difference has no effect on the results of applying the gate to the diagonal product operators (i.e. single states), but the results of applying the Pound-Overhauser XOR to a superposition may differ by phase factors from the results obtained with the quantum computing XOR.

To see how to get the same phase factors, we compute the infinitesimal generators of the two XOR's, i.e.

$$\mathbf{U}_{\text{PO}}^1 = \text{Exp}(i\pi\Theta_{\text{PO}}^1) \quad \text{where} \quad \Theta_{\text{PO}}^1 = \frac{1}{2} \begin{pmatrix} 0 & 0 & 0 & 0 \\ 0 & 0 & 0 & -i \\ 0 & 0 & 0 & 0 \\ 0 & i & 0 & 0 \end{pmatrix} \quad (25)$$

and

$$\mathbf{U}_{\text{QC}}^1 = \text{Exp}(i\pi\Theta_{\text{QC}}^1) \quad \text{where} \quad \Theta_{\text{QC}}^1 = \frac{1}{2} \begin{pmatrix} 0 & 0 & 0 & 0 \\ 0 & 1 & 0 & -1 \\ 0 & 0 & 0 & 0 \\ 0 & -1 & 0 & 1 \end{pmatrix}. \quad (26)$$

These generators may be expressed in terms of product operators as

$$\Theta_{\text{PO}}^1 = \frac{1}{2}\mathbf{I}_y^1 - \mathbf{I}_y^1\mathbf{I}_z^2 \quad (27)$$

and

$$\Theta_{\text{QC}}^1 = \frac{1}{4}\mathbf{1} - \frac{1}{2}\mathbf{I}_z^2 - \frac{1}{2}\mathbf{I}_x^1 + \mathbf{I}_x^1\mathbf{I}_z^2, \quad (28)$$

*	$\frac{1}{2}\mathbf{1}$	\mathbf{I}_x^2	\mathbf{I}_y^2	\mathbf{I}_z^2
$\frac{1}{2}\mathbf{1}$	$\frac{1}{2}\mathbf{1}$	$\mathbf{I}_x^1\mathbf{I}_x^2$	$\mathbf{I}_x^1\mathbf{I}_y^2$	\mathbf{I}_z^2
\mathbf{I}_x^1	\mathbf{I}_x^1	\mathbf{I}_x^2	\mathbf{I}_y^2	$\mathbf{I}_x^1\mathbf{I}_z^2$
\mathbf{I}_y^1	$\mathbf{I}_y^1\mathbf{I}_z^2$	$\mathbf{I}_z^1\mathbf{I}_y^2$	$-\mathbf{I}_z^1\mathbf{I}_x^2$	\mathbf{I}_y^1
\mathbf{I}_z^1	$\mathbf{I}_z^1\mathbf{I}_z^2$	$-\mathbf{I}_y^1\mathbf{I}_y^2$	$\mathbf{I}_y^1\mathbf{I}_x^2$	\mathbf{I}_z^1

Table 3: The effect of the $[XOR]_{QC}^1$ pulse sequence on all the product operators of a two-spin system (cf. Table 2).

in both of which all the terms commute with one another. The term $\frac{1}{4}\mathbf{1}$ just leads to an overall phase shift, while the term $-\frac{1}{2}\mathbf{I}_z^2$ can be cancelled with a $[\pi/2]_z^2$ rotation. It follows that the unitary transformation \mathbf{U}_{QC}^1 can be obtained with a $[-\pi]_x^{+1}$ pulse together with a $[-\pi/2]_z^2$ rotation (in either order). The effect of this $[XOR]_{QC}^1$ pulse sequence on the two-spin product operators is shown in Table 3. Comparison with Table 2 shows that the two types of XOR operations differ by swaps of $\frac{1}{2}\mathbf{1}$ with \mathbf{I}_z in those product operators that contain either of these factors, and \mathbf{I}_x with \mathbf{I}_y in all the rest.

The XOR gate together with arbitrary one-bit rotations, which one can implement via soft pulses and free precession, constitute a universal set of quantum logic gates. It is nevertheless of interest to observe that the Pound-Overhauser XOR gate generalizes directly to a conditional rotation. For example, the square root of the XOR is obtained by applying a $[\pi/2]_y^{+1}$ pulse (i.e. the same pulse needed to get the XOR, but for only half as long). For the output on the first bit, this leads to the matrix

$$\sqrt{\mathbf{U}_{PO}^1} = \frac{1}{\sqrt{2}} \begin{pmatrix} 1 & 0 & 0 & 0 \\ 0 & 1 & 0 & 1 \\ 0 & 0 & 1 & 0 \\ 0 & -1 & 0 & 1 \end{pmatrix}. \quad (29)$$

To get a unitary transformation whose matrix is that of the square root of the quantum computing XOR, i.e.

$$\sqrt{\mathbf{U}_{QC}^1} = \frac{1+i}{\sqrt{2}} \begin{pmatrix} 1-i & 0 & 0 & 0 \\ 0 & 1 & 0 & -i \\ 0 & 0 & 1-i & 0 \\ 0 & -i & 0 & 1 \end{pmatrix}, \quad (30)$$

one need only apply a $[-\pi/2]_x^{+1}$ pulse together with a $[-\pi/4]_z^2$ pulse (in either order).

Based on the matrix in Eq. (29), the effect of a $[\pi/2]_y^{+1}$ pulse on the equilibrium state should be:

$$\mathbf{I}_z^1 + \mathbf{I}_z^2 \xrightarrow{[\pi/2]_y^{+1}} \frac{1}{2}\mathbf{I}_x^1 - \mathbf{I}_x^1\mathbf{I}_z^2 + \mathbf{I}_z^1\mathbf{I}_z^2 + \frac{1}{2}\mathbf{I}_z^1 + \mathbf{I}_z^2 \quad (31)$$

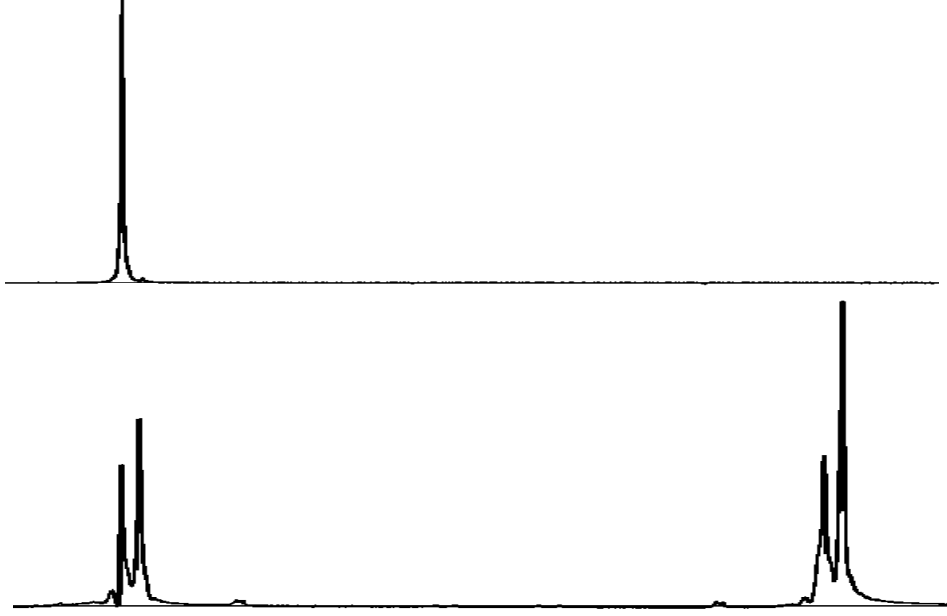


Figure 5: Validation of a Pound-Overhauser conditional rotation. The upper spectrum was collected immediately after applying the $[\pi/2]_y^{+1}$ pulse to the equilibrium state, while the lower spectrum was collected following the application of an additional hard $[\pi/2]_y^{12}$ pulse.

This gives rise to a spectrum containing a single peak at the very same frequency that the pulse was tuned to. An additional hard readout pulse produces the state

$$-\frac{1}{2}\mathbf{I}_z^1 + \mathbf{I}_z^1\mathbf{I}_x^2 + \mathbf{I}_x^1\mathbf{I}_x^2 + \frac{1}{2}\mathbf{I}_x^1 + \mathbf{I}_x^2. \quad (32)$$

The corresponding spectra are shown in Fig. 5. The general formula for a conditional rotation in terms of product operators is:

$$\begin{aligned} \mathbf{I}_z^1 &\xrightarrow{[\varphi]_y^{+1}} \cos^2(\varphi/2)\mathbf{I}_z^1 + \cos(\varphi/2)\sin(\varphi/2)(\mathbf{I}_x^1 - 2\mathbf{I}_x^1\mathbf{I}_z^2) \\ &\quad + 2\sin^2(\varphi/2)\mathbf{I}_z^1\mathbf{I}_z^2 \end{aligned} \quad (33)$$

4 The spin-coherence XOR and Toffoli gates

Due to the degree of selectivity required and the necessity for direct coupling between the spins involved, the Pound-Overhauser XOR gate can be difficult to apply. We have therefore developed the following pulse sequence, which constitutes an example of *spin-coherence double resonance* [14], and promises to be more generally useful:

$$[XOR]_{\text{SC}}^k \equiv [\pi/2]_y^k - [1/(2J_{12})] - [\pi/2]_x^k \quad (k = 1, 2) \quad (34)$$

*	$\frac{1}{2}\mathbf{1}$	\mathbf{I}_x^2	\mathbf{I}_y^2	\mathbf{I}_z^2
$\frac{1}{2}\mathbf{1}$	$\frac{1}{2}\mathbf{1}$	$-\mathbf{I}_y^1\mathbf{I}_y^2$	$\mathbf{I}_y^1\mathbf{I}_x^2$	\mathbf{I}_z^2
\mathbf{I}_x^1	\mathbf{I}_y^1	$-\mathbf{I}_y^2$	\mathbf{I}_x^2	$\mathbf{I}_y^1\mathbf{I}_z^2$
\mathbf{I}_y^1	$-\mathbf{I}_x^1\mathbf{I}_z^2$	$\mathbf{I}_z^1\mathbf{I}_x^2$	$\mathbf{I}_z^1\mathbf{I}_y^2$	$-\mathbf{I}_x^1$
\mathbf{I}_z^1	$\mathbf{I}_z^1\mathbf{I}_z^2$	$\mathbf{I}_x^1\mathbf{I}_x^2$	$\mathbf{I}_x^1\mathbf{I}_y^2$	\mathbf{I}_z^1

Table 4: The effect of the $[XOR]_{SC}^1$ pulse sequence on all the product operators of a two-spin system (cf. Tables 2 & 3).

To show that this does indeed effect the boolean XOR operation, we demonstrate that it has the same effect on the diagonal product operators as the Pound-Overhauser XOR above, e.g. for $k = 1$:

$$\begin{aligned}
 \mathbf{I}_z^1 &\xrightarrow{[\pi/2]_y^1} \mathbf{I}_x^1 \xrightarrow{[1/(2J_{12})]} 2\mathbf{I}_y^1\mathbf{I}_z^2 \xrightarrow{[\pi/2]_x^1} 2\mathbf{I}_z^1\mathbf{I}_z^2 \\
 \mathbf{I}_z^2 &\xrightarrow{[\pi/2]_y^1} \mathbf{I}_z^2 \xrightarrow{[1/(2J_{12})]} \mathbf{I}_z^2 \xrightarrow{[\pi/2]_x^1} \mathbf{I}_z^2 \\
 2\mathbf{I}_z^1\mathbf{I}_z^2 &\xrightarrow{[\pi/2]_y^1} 2\mathbf{I}_x^1\mathbf{I}_z^2 \xrightarrow{[1/(2J_{12})]} \mathbf{I}_y^1 \xrightarrow{[\pi/2]_x^1} \mathbf{I}_z^1
 \end{aligned} \tag{35}$$

Table 4 shows the effect of this gate on all the two-spin product operators. Alternatively, we can just multiply together the matrices of the three individual steps, to obtain

$$\mathbf{U}_{SC}^1 = \frac{1}{\sqrt{2}} \begin{pmatrix} 1+i & 0 & 0 & 0 \\ 0 & 0 & 0 & 1+i \\ 0 & 0 & 1-i & 0 \\ 0 & -1+i & 0 & 0 \end{pmatrix}. \tag{36}$$

We shall call this the *spin-coherence XOR gate*.

The validity of this XOR implementation is corroborated by the spectra shown in Fig. 6, which were obtained by applying this sequence to the equilibrium state followed by soft readout pulses. The infinitesimal generator of the product of the matrix in Eq. (36) with the matrix of the usual quantum computing XOR from Eq. (24) is

$$\mathbf{U}_{QC}^1 \mathbf{U}_{SC}^1 = \mathbf{Exp}(i\pi\Delta) \quad \text{where} \quad \Delta = \frac{1}{2}\mathbf{1} + \frac{1}{2}\mathbf{I}_z^1 - \frac{1}{2}\mathbf{I}_z^2. \tag{37}$$

Together with the fact that \mathbf{U}_{QC}^1 is self-inverse and commutes with $\mathbf{Exp}(i\pi\mathbf{I}_z^2/2)$, this generator shows that the phases of the nonzero components can again be equalized by composing this pulse sequence with suitable z -rotations, namely $[\pi/2]_z^2 - [XOR]_{SC}^1 - [-\pi/2]_z^1$.

We have also developed a pulse sequence, analogous to the above $[XOR]_{SC}^k$ sequence, which transforms the longitudinal spin states of a three-spin system according to the truth table of the well-known Toffoli gate [15]. We call this the

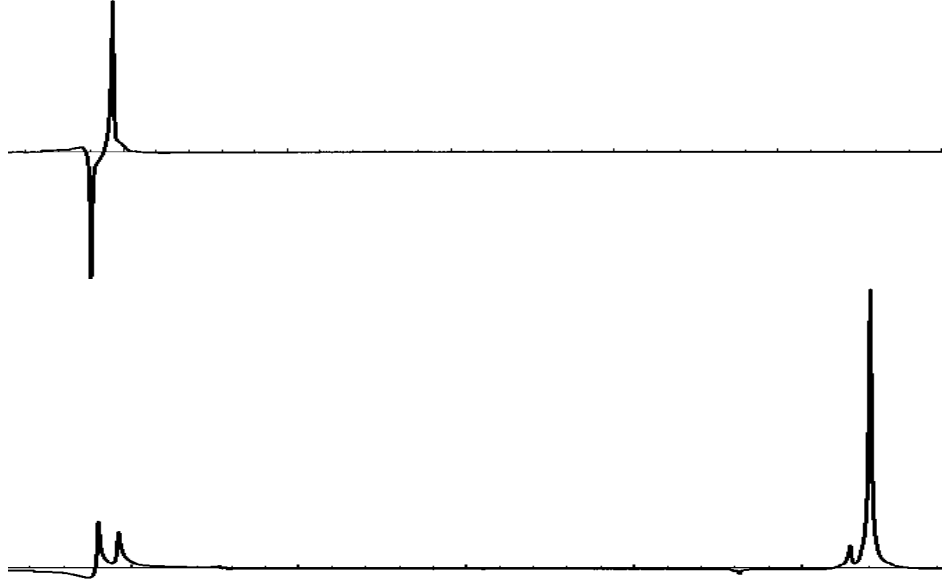


Figure 6: The spectra obtained from readout pulses on the two spins, following a $[XOR]_{\text{SC}}^1$ pulse sequence applied to the equilibrium state (see text).

Toffoli pulse sequence:

$$[TOF]_{\text{SC}}^k \equiv [\pi/2]_y^k - [1/(4J)] - [\pi/2]_y^k - [1/(4J)] - [-\pi/2]_x^k - [1/(4J)] - [-\pi/2]_x^k \quad (38)$$

This pulse sequence assumes that the coupling constants $J_{k\ell}$ and J_{km} have the same value J , which can always be arranged by inverting the spin whose coupling constant with k is greater using a soft $[\pi]$ pulse part way through each delay. This changes the sign of the effective coupling constant, so that the time-average coupling constant can be given any desired value between the original coupling constant and its negative.

If we place the output on the first spin ($k = 1$), the matrix of the above Toffoli sequence can be shown to be:

$$\mathbf{V}_{\text{SC}}^1 = -\frac{1}{\sqrt{2}} \begin{pmatrix} 1+i & 0 & 0 & 0 & 0 & 0 & 0 & 0 \\ 0 & i & 0 & 0 & 0 & 0 & 0 & 0 \\ 0 & 0 & i & 0 & 0 & 0 & 0 & 0 \\ 0 & 0 & 0 & 0 & 0 & 0 & 0 & 1-i \\ 0 & 0 & 0 & 0 & 1-i & 0 & 0 & 0 \\ 0 & 0 & 0 & 0 & 0 & -i & 0 & 0 \\ 0 & 0 & 0 & 0 & 0 & 0 & -i & 0 \\ 0 & 0 & 0 & -1-i & 0 & 0 & 0 & 0 \end{pmatrix} \quad (39)$$

This is easily seen to act upon the density matrices associated with single states

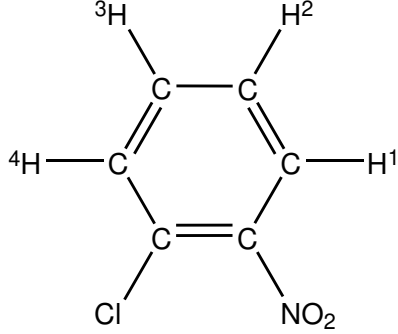


Figure 7: The chemical structure of 1-chloro-2-nitro-benzene, which was used to validate the spin-coherence implementation of the Toffoli gate by applying the $[TOF]_{SC}^1$ sequence to hydrogen atoms 1–3. The relevant coupling constants among these atoms are $J_{12} = 8.0$ Hz., $J_{13} = 1.5$ Hz., and $J_{14} \leq 0.1$ Hz., and $J_{23} = 7.0$ Hz.

as

$$\begin{aligned} & \mathbf{V}_{SC}^{1\dagger} |\epsilon_1, \epsilon_2, \epsilon_3\rangle \langle \epsilon_1, \epsilon_2, \epsilon_3| \mathbf{V}_{SC}^1 \\ &= |\epsilon_1 \oplus (\epsilon_2 \wedge \epsilon_3), \epsilon_2, \epsilon_3\rangle \langle \epsilon_1 \oplus (\epsilon_2 \wedge \epsilon_3), \epsilon_2, \epsilon_3| \end{aligned} \quad (40)$$

(where the “ \wedge ” denotes the boolean AND operation). Unlike the XOR sequence, however, the Toffoli sequence does not simply permute the diagonal product operators; instead, it results in a sum of such diagonal operators, e.g.

$$\begin{aligned} \mathbf{I}_z^1 & \xrightarrow{[\pi/2]_y^1} \mathbf{I}_x^1 \\ & \xrightarrow{[1/(4J)]} \frac{1}{2} \mathbf{I}_x^1 + \mathbf{I}_y^1 \mathbf{I}_z^2 + \mathbf{I}_y^1 \mathbf{I}_z^3 - 2 \mathbf{I}_x^1 \mathbf{I}_z^2 \mathbf{I}_z^3 \\ & \xrightarrow{[\pi/2]_y^1} -\frac{1}{2} \mathbf{I}_z^1 + \mathbf{I}_y^1 \mathbf{I}_z^2 + \mathbf{I}_y^1 \mathbf{I}_z^3 + 2 \mathbf{I}_z^1 \mathbf{I}_z^2 \mathbf{I}_z^3 \\ & \xrightarrow{[1/(4J)]} -\frac{1}{2} \mathbf{I}_z^1 - \frac{1}{2} \mathbf{I}_x^1 - 2 \mathbf{I}_x^1 \mathbf{I}_z^2 \mathbf{I}_z^3 + 2 \mathbf{I}_z^1 \mathbf{I}_z^2 \mathbf{I}_z^3 \\ & \xrightarrow{[-\pi/2]_x^1} -\frac{1}{2} \mathbf{I}_y^1 - \frac{1}{2} \mathbf{I}_x^1 - 2 \mathbf{I}_x^1 \mathbf{I}_z^2 \mathbf{I}_z^3 + 2 \mathbf{I}_y^1 \mathbf{I}_z^2 \mathbf{I}_z^3 \\ & \xrightarrow{[1/(4J)]} -\frac{1}{2} \mathbf{I}_y^1 - \mathbf{I}_y^1 \mathbf{I}_z^2 - \mathbf{I}_y^1 \mathbf{I}_z^3 + 2 \mathbf{I}_y^1 \mathbf{I}_z^2 \mathbf{I}_z^3 \\ & \xrightarrow{[-\pi/2]_x^1} \frac{1}{2} \mathbf{I}_z^1 + \mathbf{I}_z^1 \mathbf{I}_z^2 + \mathbf{I}_z^1 \mathbf{I}_z^3 - 2 \mathbf{I}_z^1 \mathbf{I}_z^2 \mathbf{I}_z^3. \end{aligned} \quad (41)$$

Similar calculations lead to the following complete list:

$$\begin{aligned}
\mathbf{I}_z^1 &\xrightarrow{[TOF]_{SC}^1} \frac{1}{2}\mathbf{I}_z^1 + \mathbf{I}_z^1\mathbf{I}_z^2 + \mathbf{I}_z^1\mathbf{I}_z^3 - 2\mathbf{I}_z^1\mathbf{I}_z^2\mathbf{I}_z^3 \\
\mathbf{I}_z^2 &\xrightarrow{[TOF]_{SC}^1} \mathbf{I}_z^2 \\
\mathbf{I}_z^3 &\xrightarrow{[TOF]_{SC}^1} \mathbf{I}_z^3 \\
2\mathbf{I}_z^1\mathbf{I}_z^2 &\xrightarrow{[TOF]_{SC}^1} \frac{1}{2}\mathbf{I}_z^1 + \mathbf{I}_z^1\mathbf{I}_z^2 - \mathbf{I}_z^1\mathbf{I}_z^3 + 2\mathbf{I}_z^1\mathbf{I}_z^2\mathbf{I}_z^3 \\
2\mathbf{I}_z^1\mathbf{I}_z^3 &\xrightarrow{[TOF]_{SC}^1} \frac{1}{2}\mathbf{I}_z^1 - \mathbf{I}_z^1\mathbf{I}_z^2 + \mathbf{I}_z^1\mathbf{I}_z^3 + 2\mathbf{I}_z^1\mathbf{I}_z^2\mathbf{I}_z^3 \\
2\mathbf{I}_z^2\mathbf{I}_z^3 &\xrightarrow{[TOF]_{SC}^1} 2\mathbf{I}_z^2\mathbf{I}_z^3 \\
4\mathbf{I}_z^1\mathbf{I}_z^2\mathbf{I}_z^3 &\xrightarrow{[TOF]_{SC}^1} -\frac{1}{2}\mathbf{I}_z^1 + \mathbf{I}_z^1\mathbf{I}_z^2 + \mathbf{I}_z^1\mathbf{I}_z^3 + 2\mathbf{I}_z^1\mathbf{I}_z^2\mathbf{I}_z^3
\end{aligned} \tag{42}$$

Once again, these claims can be corroborated by using the matrix in Eq. (39) to predict the result of applying the $[TOF]_{SC}^1$ sequence to the equilibrium state, and then verifying that the results are consistent with the spectra collected after appropriate readout pulses. These spectra are rather complicated, however, and hence we shall simply show the result of applying the readout pulse to the first spin. The molecule used for these experiments, 1-chloro-2-nitro-benzene, is actually a four-spin system, thus enabling us to also demonstrate that we can apply quantum logic gates to subsets of spins, given sufficient frequency resolution. This spectrum is shown in Fig. 8, along with the spectra obtained by applying the same readout pulse to the four diagonal product operators (prepared by the gradient-pulse techniques described earlier) for comparison. The fact that just one of the four peaks due to the first spin has been inverted by the Toffoli sequence is a direct reflection of the fact that the population difference of the first spin has been inverted in just those molecules wherein the other two spins were “up”.

In order to equalize the phase factors, we compute the infinitesimal generator of the product of the matrix \mathbf{V}_{SC}^1 for the $[TOF]_{SC}^1$ gate shown in Eq. (39) with the desired matrix \mathbf{V}_{QC}^1 (consisting of ones at all the same nonzero locations):

$$\begin{aligned}
\mathbf{Exp}(i\pi\Delta) &= \mathbf{V}_{QC}^1 \mathbf{V}_{SC}^1 \quad \text{where} \\
\Delta &= \frac{1}{8}\mathbf{1} - \mathbf{I}_z^1 - \frac{1}{4}\mathbf{I}_z^2 - \frac{1}{4}\mathbf{I}_z^3 - \frac{1}{2}\mathbf{I}_z^1\mathbf{I}_z^2 - \frac{1}{2}\mathbf{I}_z^1\mathbf{I}_z^3 + \frac{1}{2}\mathbf{I}_z^2\mathbf{I}_z^3
\end{aligned} \tag{43}$$

These are all z -rotations of one kind or another, and hence can all be readily obtained from the three-spin analogues of the implementations introduced above for a two-spin system (save possibly for the rotation whose generator is $\mathbf{I}_z^2\mathbf{I}_z^3$, which will require a relay sequence if these spins are not directly coupled [14]).

The Toffoli gate is known to be universal for classical computation, and hence the existence of this pulse sequence shows that any boolean function can be implemented in NMR via soft pulses selective for single spins. A Pound-Overhauser implementation of the Toffoli gate is also possible, but we have not yet done the experiments to demonstrate this.

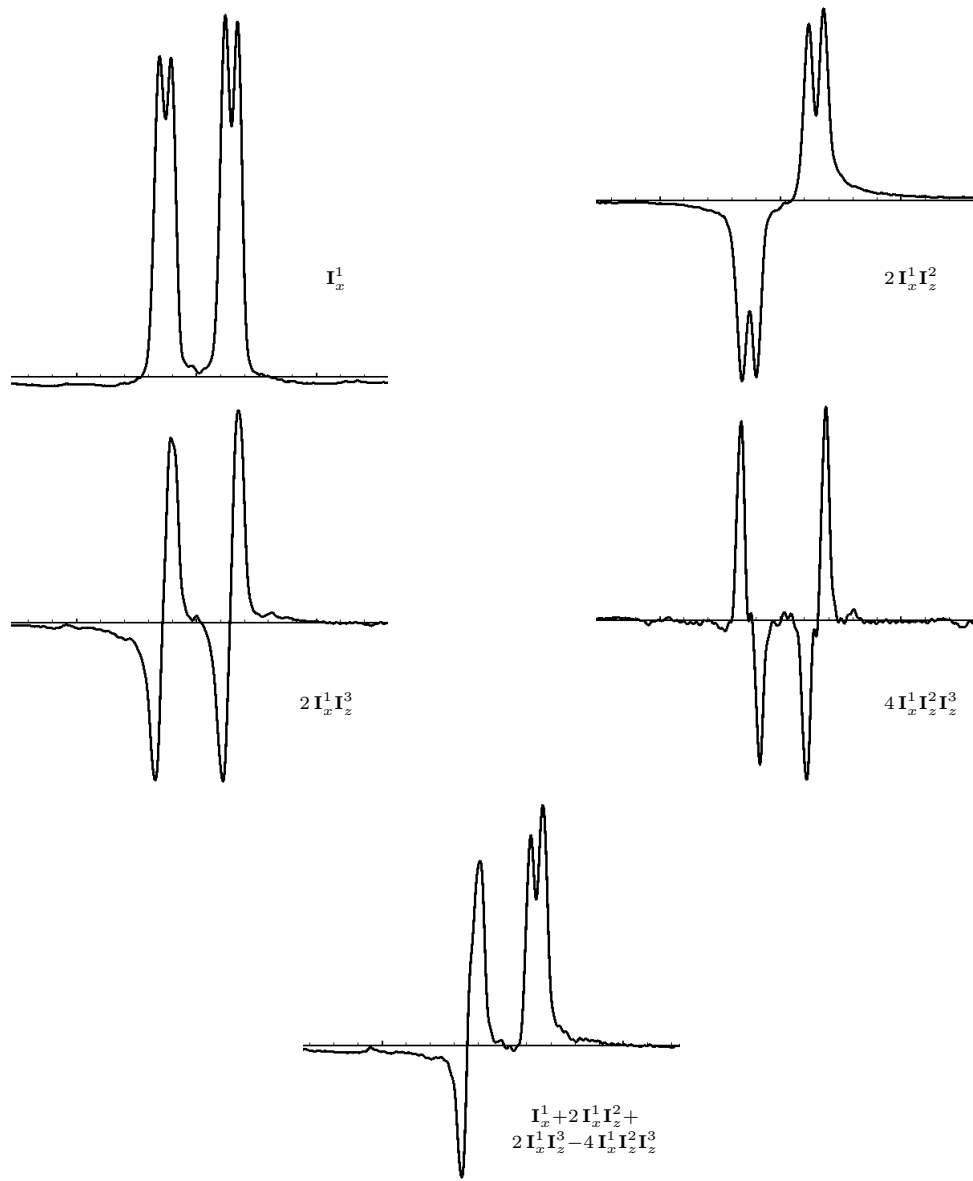


Figure 8: The spectra of 1-chloro-2-nitro-benzene obtained following a $[\pi/2]_y^1$ readout pulse to the four diagonal product operators \mathbf{I}_z^1 , $2\mathbf{I}_z^1\mathbf{I}_z^2$, $2\mathbf{I}_z^1\mathbf{I}_z^3$ and $2\mathbf{I}_z^1\mathbf{I}_z^2\mathbf{I}_z^3$, as well as to the result of applying the $[TOF]_{SC}^1$ pulse sequence to the equilibrium state (see text).

5 Superpositions of pseudo-spinors

If one generates all three of the states \mathbf{I}_z^1 , \mathbf{I}_z^2 and $2\mathbf{I}_z^1\mathbf{I}_z^2$ simultaneously in the same sample, one obtains the density matrix

$$\mathbf{I}_z^1 + \mathbf{I}_z^2 + 2\mathbf{I}_z^1\mathbf{I}_z^2 = \begin{pmatrix} \frac{3}{2} & 0 & 0 & 0 \\ 0 & -\frac{1}{2} & 0 & 0 \\ 0 & 0 & -\frac{1}{2} & 0 \\ 0 & 0 & 0 & -\frac{1}{2} \end{pmatrix} \quad (44)$$

This matrix shifts to

$$\begin{pmatrix} 2 & 0 & 0 & 0 \\ 0 & 0 & 0 & 0 \\ 0 & 0 & 0 & 0 \\ 0 & 0 & 0 & 0 \end{pmatrix}, \quad (45)$$

which can in turn be factored into the product of a pseudo-spinor with its conjugate,

$$2|00\rangle\langle 00| \equiv 2 \begin{pmatrix} 1 \\ 0 \\ 0 \\ 0 \end{pmatrix} (1 \quad 0 \quad 0 \quad 0). \quad (46)$$

Therefore, the expression $\mathbf{I}_z^1 + \mathbf{I}_z^2 + 2\mathbf{I}_z^1\mathbf{I}_z^2$ in Eq. (44) represents a pseudo-pure state in product operator notation.

The following RF and gradient pulse sequence transforms the equilibrium state of a two-spin system into this pseudo-pure state:

$$\begin{aligned} & \mathbf{I}_z^1 + \mathbf{I}_z^2 \\ \xrightarrow{[\pi/3]_x^2} & \mathbf{I}_z^1 + \mathbf{I}_z^2/2 - \mathbf{I}_y^2\sqrt{3}/2 \\ \xrightarrow{[\text{grad}]_z} & \mathbf{I}_z^1 + \mathbf{I}_z^2/2 \\ \xrightarrow{[\pi/4]_x^1} & \mathbf{I}_z^1/\sqrt{2} + \mathbf{I}_z^2/2 - \mathbf{I}_y^1/\sqrt{2} \\ \xrightarrow{[1/(2J_{12})]} & \mathbf{I}_z^1/\sqrt{2} + \mathbf{I}_z^2/2 + \sqrt{2}\mathbf{I}_x^1\mathbf{I}_z^2 \\ \xrightarrow{[-\pi/4]_y^1} & \mathbf{I}_z^1/2 + \mathbf{I}_z^2/2 - \mathbf{I}_x^1/2 + \mathbf{I}_x^1\mathbf{I}_z^2 + \mathbf{I}_z^1\mathbf{I}_z^2 \\ \xrightarrow{[\text{grad}]_z} & \mathbf{I}_z^1/2 + \mathbf{I}_z^2/2 + \mathbf{I}_z^1\mathbf{I}_z^2 \end{aligned} \quad (47)$$

Subsequently, any of the four *basic* pseudo-pure states (with a density matrix shifting to a matrix with a single nonzero element on the diagonal) can be obtained by means of soft $[\pi]$ pulses (which perform the NOT operation on the

spins). In terms of product operators, these can be written as:

$$\begin{aligned} 2|00\rangle\langle 00| - \frac{1}{2}\mathbf{1} &= \mathbf{I}_z^1 + \mathbf{I}_z^2 + 2\mathbf{I}_z^1\mathbf{I}_z^2 \\ 2|01\rangle\langle 01| - \frac{1}{2}\mathbf{1} &= \mathbf{I}_z^1 - \mathbf{I}_z^2 - 2\mathbf{I}_z^1\mathbf{I}_z^2 \\ 2|10\rangle\langle 10| - \frac{1}{2}\mathbf{1} &= -\mathbf{I}_z^1 + \mathbf{I}_z^2 - 2\mathbf{I}_z^1\mathbf{I}_z^2 \\ 2|11\rangle\langle 11| - \frac{1}{2}\mathbf{1} &= -\mathbf{I}_z^1 - \mathbf{I}_z^2 + 2\mathbf{I}_z^1\mathbf{I}_z^2 \end{aligned} \quad (48)$$

The factor of 1/2 difference between the last line of Eq. (47) and the first line in Eq. (48) is due to a 25% loss of total polarization during the gradient pulses. Note that by changing the sign of either of the two $[\pi/4]$ rotations in Eq. (47), we can generate the state $\mathbf{I}_z^1 + \mathbf{I}_z^2 - 2\mathbf{I}_z^1\mathbf{I}_z^2$. This is the *negative* of last state in Eq. (48), which means the polarization of the sample (i.e. the sign of the nonzero element after shifting the density matrix) is inverted between the two states. The negatives of all four states in Eq. (48) can likewise be interconverted by soft $[\pi]$ pulses, but none of these states can be converted to its negative by means of RF pulses. Whether we use the four basis states in Eq. (48) or their negatives is irrelevant for computational purposes.

To validate that with the use of a $[\pi/4]_y^1$ instead of a $[-\pi/4]_y^1$ pulse in Eq. (47), we have actually created the expected state $\mathbf{I}_z^1 + \mathbf{I}_z^2 - 2\mathbf{I}_z^1\mathbf{I}_z^2$, we consider the spectra that are obtained after applying soft readout pulses to each of the two spins, i.e.

$$\mathbf{I}_z^1 + \mathbf{I}_z^2 - 2\mathbf{I}_z^1\mathbf{I}_z^2 \xrightarrow{[\pi/2]_y^1} \mathbf{I}_x^1 + \mathbf{I}_z^2 - 2\mathbf{I}_x^1\mathbf{I}_z^2 \quad (49)$$

and

$$\mathbf{I}_z^1 + \mathbf{I}_z^2 - 2\mathbf{I}_z^1\mathbf{I}_z^2 \xrightarrow{[\pi/2]_y^2} \mathbf{I}_z^1 + \mathbf{I}_x^2 - 2\mathbf{I}_z^1\mathbf{I}_x^2. \quad (50)$$

This creates the difference of an in-phase with an anti-phase state in both cases, so that the associated spectra consist of single peaks at the leftmost position of the corresponding doublet. These spectra are shown in Fig. 9.

The density matrices generated by these readout pulses can be written in terms of the associated pseudo-spinors as

$$\begin{aligned} \frac{1}{2}\mathbf{1} - (|0\rangle - |1\rangle)|1\rangle\langle 0| - \langle 1| |1\rangle &= \mathbf{I}_x^1 + \mathbf{I}_z^2 - 2\mathbf{I}_x^1\mathbf{I}_z^2 \\ \frac{1}{2}\mathbf{1} - |1\rangle(|0\rangle - |1\rangle)\langle 1| - \langle 0| |1\rangle &= \mathbf{I}_z^1 + \mathbf{I}_x^2 - 2\mathbf{I}_z^1\mathbf{I}_x^2. \end{aligned} \quad (51)$$

In other words, each readout pulse puts the corresponding spin into a superposition over its longitudinal states. We can create a superposition over both spins by performing the two readout pulses in rapid succession, or with a single “hard” pulse (which takes only a small fraction of the time required for a soft pulse), i.e.

$$\frac{1}{2}\mathbf{1} - 2|11\rangle\langle 11| \xrightarrow{[\pi/2]_y^{12}} \mathbf{I}_x^1 + \mathbf{I}_x^2 - 2\mathbf{I}_x^1\mathbf{I}_x^2 \quad (52)$$

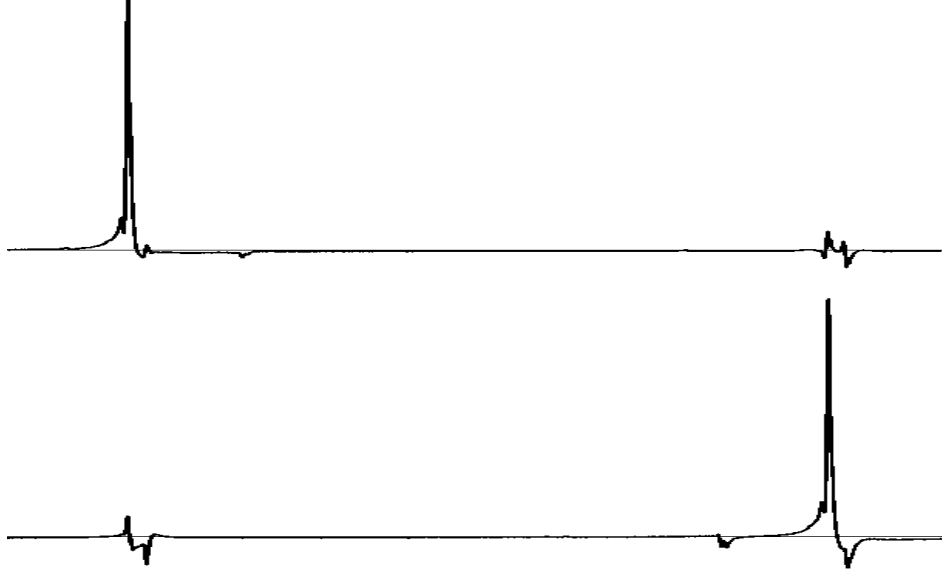


Figure 9: Two experimental NMR spectra of 2,3-dibromo-thiophene, which corroborate the creation of the pseudo-pure state $\mathbf{I}_z^1 + \mathbf{I}_z^2 - 2\mathbf{I}_z^1\mathbf{I}_z^2$ via readout pulses selective for the first (above) and second (below) spins (see text).

Since $2\mathbf{I}_x^1\mathbf{I}_x^2$ does not contribute to the signal, the spectrum in this case consists of a pair of in-phase doublets, exactly like that shown in Fig. 1.

In NMR computing, superpositions over the basic pseudo-pure states are always associated with nonzero off-diagonal coherences in the density matrix. The product operator above, for example, represents the matrix

$$\begin{aligned}
 \mathbf{I}_x^1 + \mathbf{I}_x^2 - 2\mathbf{I}_x^1\mathbf{I}_x^2 &= \frac{1}{2}(\mathbf{1} - (|0\rangle - |1\rangle)(|0\rangle - |1\rangle) \\
 &\quad (\langle 0| - \langle 1|)(\langle 0| - \langle 1|)) \\
 &= \frac{1}{2} \begin{pmatrix} 0 & 1 & 1 & -1 \\ 1 & 0 & -1 & 1 \\ 1 & -1 & 0 & 1 \\ -1 & 1 & 1 & 0 \end{pmatrix} \quad (53)
 \end{aligned}$$

Since the corresponding pseudo-spinor can be factored into a product of one-spin pseudo-spinors (as shown), it represents an “umentangled” state.

The fact that we have successfully prepared a pseudo-pure state, and our spin-coherence XOR gate, can both be further corroborated by putting them together. The resulting spectra are shown in Fig. 10. We have also confirmed that the superposition created by applying a soft $[\pi/2]_y^1$ pulse to the $\mathbf{I}_z^1 + \mathbf{I}_z^2 + 2\mathbf{I}_z^1\mathbf{I}_z^2$ state, namely $(|0\rangle + |1\rangle)|0\rangle$, is changed by only inconsequential phase factors on applying the $[XOR]_{SC}^1$ sequence to it. These phase changes can nevertheless be made visible by applying a further $[\pi/2]_y^2$ readout pulse to the

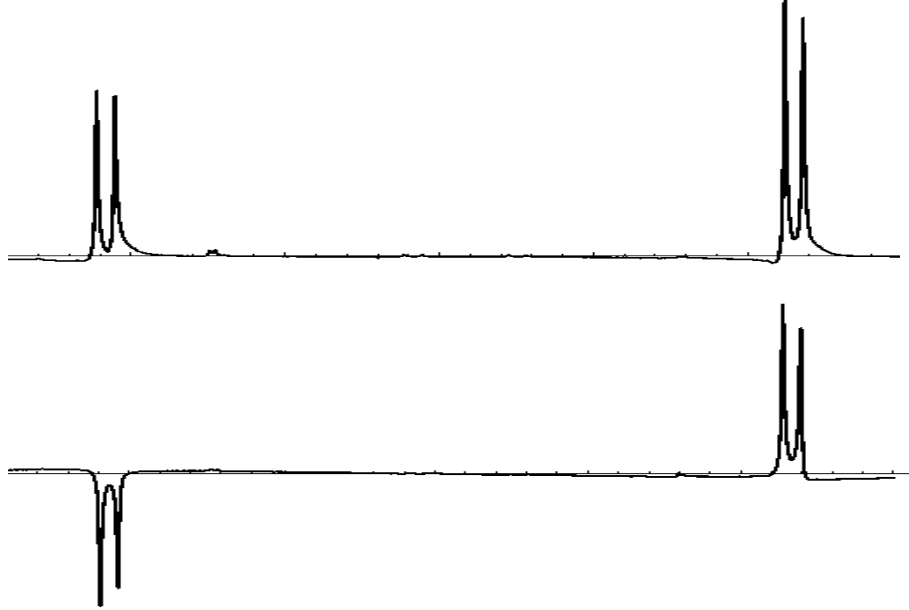


Figure 10: The effect of applying the $[XOR]_{SC}^1$ pulse sequence to the pseudo-pure state $\mathbf{I}_z^1 + \mathbf{I}_z^2 - 2\mathbf{I}_z^1\mathbf{I}_z^2$ to get $-\mathbf{I}_z^1 + \mathbf{I}_z^2 + 2\mathbf{I}_z^1\mathbf{I}_z^2$. This is clearly seen from the change in sign of the first in-phase doublet following a hard $[\pi/2]_y^{12}$ pulse, before (above) and after (below) the XOR.

result, as shown in Fig. 11 and described in its caption. Finally, we consider the result of applying the $[XOR]_{SC}^2$ gate, with its output on the other spin, to this same one-spin superposition. As is well-known, this creates an “entangled” state

$$\mathbf{I}_x^1 + \mathbf{I}_z^2 + 2\mathbf{I}_x^2\mathbf{I}_z^2 \xrightarrow{[XOR]_{SC}^2} 2\mathbf{I}_x^1\mathbf{I}_x^2 - 2\mathbf{I}_y^1\mathbf{I}_y^2 + 2\mathbf{I}_z^2\mathbf{I}_z^2, \quad (54)$$

or equivalently:

$$\frac{1}{2}(-\mathbf{1} + (|00\rangle + |10\rangle)) \xrightarrow{[XOR]_{SC}^2} \frac{1}{2}(-\mathbf{1} + (|00\rangle + |11\rangle)) \quad (55)$$

$$(|00\rangle + |10\rangle) \quad (|00\rangle + |11\rangle)$$

In this case the transverse magnetization corresponds to a *double-quantum coherence*,

$$2\mathbf{I}_x^1\mathbf{I}_x^2 - 2\mathbf{I}_y^1\mathbf{I}_y^2 = \begin{pmatrix} 0 & 0 & 0 & 1 \\ 0 & 0 & 0 & 0 \\ 0 & 0 & 0 & 0 \\ 1 & 0 & 0 & 0 \end{pmatrix}, \quad (56)$$

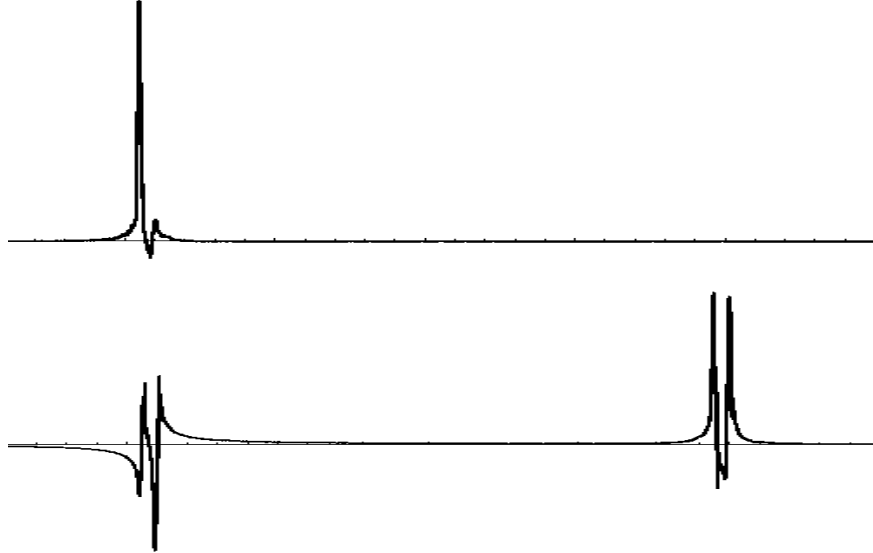


Figure 11: The result of applying the $[XOR]_{SC}^1$ sequence to the one-spin superposition created by applying a $[\pi/2]_y^1$ pulse to the pseudo-pure state $\mathbf{I}_z^1 + \mathbf{I}_z^2 + 2\mathbf{I}_z^1\mathbf{I}_z^2$, to get $\mathbf{I}_y^1 + \mathbf{I}_z^2 + 2\mathbf{I}_y^1\mathbf{I}_z^2$ (above). This is then further confirmed with an additional $[\pi/2]_y^2$ readout pulse to get $\mathbf{I}_y^1 + \mathbf{I}_x^2 + 2\mathbf{I}_y^1\mathbf{I}_x^2$, which consists of two in-phase doublets that are 90° out-of-phase with each other, so that one doublet appears as a pair of dispersive peaks whenever the other is phased to be an absorptive pair (below).

which precesses at twice the rate of the single-quantum terms, but produces no observable magnetization. The most direct way to confirm the creation of this double-quantum coherence is via a *gradient echo* experiment. In this technique, one applies a $+z$ -gradient for a period of $1/(2J_{12})$, followed by a soft $[-\pi/2]_y^2$ pulse, and then an *inverse* $-z$ -gradient. The double-quantum coherence dephases at twice the rate of a single-quantum coherence, but even though no macroscopic magnetization remains at the end of the $+z$ -gradient, the microscopic coherence $2\mathbf{I}_x^1\mathbf{I}_x^2$ is still converted to $2\mathbf{I}_x^1\mathbf{I}_z^2$ by the $[-\pi/2]_y^2$ pulse. This term then rephases under the $-z$ -gradient at the usual rate for a single-quantum coherence, while at the same time evolving under coupling to \mathbf{I}_y^1 . This in turn results in observable transverse magnetization, which reaches its maximum after a period of $1/J_{12}$. The double-quantum echo appears after twice the time of the echo due to the rephasing of the (residual!) single-quantum coherence. If we collect the data for a spectrum starting right after the $[-\pi/2]_y^2$ pulse, we observe the expected anti-phase doublet (Fig. 12).

For completeness, Table 5 gives the coefficients of the seven diagonal product operators in the eight basic pseudo-pure states of a three-spin system. A pulse

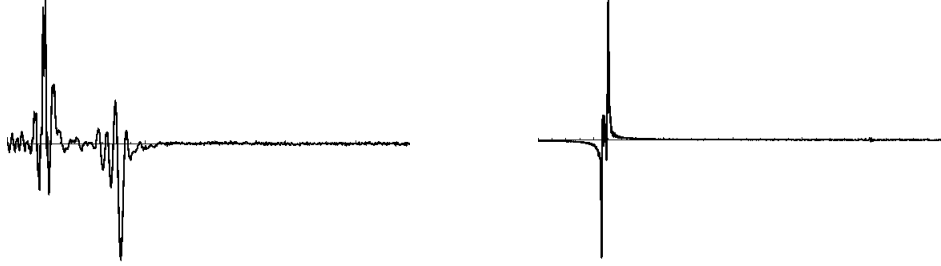


Figure 12: Time-domain echo of the double-quantum coherence characteristic of an ‘entangled’ pseudo-spinor (left), together with the corresponding frequency-domain spectrum (right). The first echo, due to residual single-quantum coherence, occurs in half the time required for the double-quantum echo to form (see text).

sequence and gradient sequence that generates the $|000\rangle$ state is:

$$\begin{aligned}
 & \mathbf{I}_z^1 + \mathbf{I}_z^2 + \mathbf{I}_z^3 \\
 \xrightarrow{[5\pi/12]_y^1 - [\pi/3]_y^2 - [\text{grad}]_z} & \frac{1}{4}\mathbf{I}_z^1 + \frac{1}{2}\mathbf{I}_z^2 + \mathbf{I}_z^3 \\
 \xrightarrow{[\pi/4]_y^2 - [1/(2J_{12})] - [-\pi/4]_x^2 - [\text{grad}]_z} & \frac{1}{4}\mathbf{I}_z^1 + \frac{1}{4}\mathbf{I}_z^2 + \mathbf{I}_z^3 + \frac{1}{2}\mathbf{I}_z^1\mathbf{I}_z^2 \\
 \xrightarrow{[\pi/4]_y^3 - [1/(2J)] - [\pi/4]_y^3 - [\text{grad}]_z} & \frac{1}{4}\mathbf{I}_z^1 + \frac{1}{4}\mathbf{I}_z^2 + \frac{1}{2}\mathbf{I}_z^3 + \frac{1}{2}\mathbf{I}_z^1\mathbf{I}_z^2 + \\
 & 2\mathbf{I}_z^1\mathbf{I}_z^2\mathbf{I}_z^3 \\
 \xrightarrow{[\pi/4]_y^3 - [1/(4J)] - [\pi/4]_x^3 - [\text{grad}]_z} & \frac{1}{4}\mathbf{I}_z^1 + \frac{1}{4}\mathbf{I}_z^2 + \frac{1}{4}\mathbf{I}_z^3 + \frac{1}{2}\mathbf{I}_z^1\mathbf{I}_z^2 + \\
 & \frac{1}{2}\mathbf{I}_z^1\mathbf{I}_z^3 + \frac{1}{2}\mathbf{I}_z^2\mathbf{I}_z^3 + \mathbf{I}_z^1\mathbf{I}_z^2\mathbf{I}_z^3
 \end{aligned} \tag{57}$$

In this sequence, $[1/(2J_{12})]$ stands for a coupling evolution period with the coupling constants J_{13} and J_{23} averaged to zero by a $[\pi]$ pulse on the third spin, while $[1/(2J)]$ and $[1/(4J)]$ are evolution periods with J_{12} averaged to zero and J_{13} , J_{23} averaged to the same value J .

6 Conclusions

We have demonstrated that nuclear magnetic resonance spectroscopy provides an experimentally accessible paradigm for quantum computing. In particular, the results given in this paper include the first physical implementations of all the basic quantum logic gates, including the XOR and Toffoli gates, which have up to now been largely theoretical constructions. We have further shown that one can actually prepare a macroscopic ensemble of weakly polarized spin systems in a pseudo-pure state, which can be described by a spinor just like a true pure state, and confirmed that one can put these states into the equivalent

Spinor	\mathbf{I}_z^1	\mathbf{I}_z^2	\mathbf{I}_z^3	$2\mathbf{I}_z^1\mathbf{I}_z^2$	$2\mathbf{I}_z^1\mathbf{I}_z^3$	$2\mathbf{I}_z^2\mathbf{I}_z^3$	$4\mathbf{I}_z^1\mathbf{I}_z^2\mathbf{I}_z^3$
$ 000\rangle$	1	1	1	1	1	1	1
$ 001\rangle$	1	1	-1	1	-1	-1	-1
$ 010\rangle$	1	-1	1	-1	1	-1	-1
$ 011\rangle$	1	-1	-1	-1	-1	1	1
$ 100\rangle$	-1	1	1	-1	-1	1	-1
$ 101\rangle$	-1	1	-1	-1	1	-1	1
$ 110\rangle$	-1	-1	1	1	-1	-1	1
$ 111\rangle$	-1	-1	-1	1	1	1	-1

Table 5: Table of coefficients of the seven diagonal product operators corresponding to each basic pseudo-spinor for a three-spin system.

of entangled superpositions. Finally, we have shown how the state of the system can be efficiently determined from spectra collected following suitable readout pulses.

These operations provide essentially all the ingredients needed to efficiently emulate a true quantum computer by NMR spectroscopy. Nevertheless, as has recently been forcefully pointed out [16], the population difference for any single spin that results from preparing a pseudo-pure state by averaging over unitary transformations of the thermal equilibrium state falls off as at least $n/(2^n - 1)$ with the number of spins n (cf. [12]). This means that the signal-to-noise in the spectra decreases exponentially with n , which precludes extending this emulation beyond 8 – 12 spins in the foreseeable future. Subject to these same limitations, however, an NMR computer is also able to directly estimate the expectation values of its observables [5]. While this does not lead to any asymptotic performance gains over what can be done with a quantum computer, it remains a potentially significant advantage. We conclude that the computational potential of NMR spectroscopy, and of ensemble quantum computing more generally, has yet to be fully explored.

Acknowledgements

This work was supported by NSF/DMR 9357603 to D.G.C., and by NSF/MCB 9527181 to T.F.H. We thank Profs. Robert Griffin, Tommaso Toffoli and Gerhard Wagner for their encouragement of our efforts.

References

[1] C. Bennett. Quantum information and computation. *Physics Today*, October:24–30, 1995.

- [2] G. Brassard. A quantum jump in computer science. In J. van Leeuwen, editor, *Computer Science Today*, volume 1000 of *Lect. Notes Comput. Sci.*, pages 1–14. Springer-Verlag, 1995.
- [3] D. Canet. *Nuclear Magnetic Resonance: Concepts and Methods*. J. Wiley & Sons, 1996.
- [4] D. G. Cory, A. F. Fahmy, and T. F. Havel. Nuclear magnetic resonance spectroscopy: An experimentally accessible paradigm for quantum computing. In *Proceedings of the Fourth Workshop on Physics and Computation*. New England Complex Systems Institute, Boston, MA, 1996.
- [5] D. G. Cory, A. F. Fahmy, and T. F. Havel. Ensemble quantum computing by nuclear magnetic resonance spectroscopy. *Proc. Natl. Acad. Sci.*, 94:1634–1639, 1997.
- [6] D. P. DiVincenzo. Quantum computation. *Science*, 270:255–261, 1995.
- [7] R. R. Ernst, G. Bodenhausen, and A. Wokaun. *Principles of Nuclear Magnetic Resonance in One and Two Dimensions*. Oxford Univ. Press, U.K., 1987.
- [8] T. C. Farrar and J. E. Harriman. *Density Matrix Theory and its Applications in NMR Spectroscopy (2nd ed.)*. Farragut Press, Madison, WI, 1995.
- [9] N. A. Gershenfeld and I. L. Chuang. Bulk spin-resonance quantum computation. *Science*, 275:350–356, 1997.
- [10] N. A. Gershenfeld, I. L. Chuang, and S. Lloyd. Bulk quantum computation. In *Proceedings of the Fourth Workshop on Physics and Computation*. New England Complex Systems Institute, Boston, MA, 1996.
- [11] M. Goldman. *Quantum Description of High-Resolution NMR in Liquids*. Clarendon Press, Oxford, U.K., 1988.
- [12] E. Knill, I. Chuang and R. Laflamme. *Effective pure states for bulk quantum computation*. LANL preprint quant-ph/9706053.
- [13] G. D. Mateescu and A. Valeriu. *2D NMR: Density Matrix and Product Operator Treatment*. Prentice Hall, Englewood Cliffs, NJ, 1993.
- [14] C. P. Slichter. *Principles of Magnetic Resonance (3rd. ed.)*. Springer-Verlag, 1990.
- [15] T. Toffoli. Reversible computing. In J. W. de Bakker and J. van Leeuwen, editors, *Automata, Languages and Programming*, pages 632–644. Springer-Verlag, 1980.
- [16] W. S. Warren. NMR computing: Tool or toy? *Science*, 1997. In press.